Comparison of Wind Power Converter Reliability with Low-Speed and Medium-Speed Permanent-Magnet Synchronous Generators

Zhou, Dao; Blaabjerg, Frede; Franke, Toke; Tonnes, Michael; Lau, Mogens

Published in:
I E E E Transactions on Industrial Electronics

DOI (link to publication from Publisher):
10.1109/TIE.2015.2447502

Publication date:
2015

Document Version
Accepted author manuscript, peer reviewed version

Comparison of Wind Power Converters Reliability with Low-Speed and Medium-Speed Permanent-Magnet Synchronous Generators

Dao Zhou, *Member, IEEE*, Frede Blaabjerg, *Fellow, IEEE*, Toke Franke, *Member, IEEE*, Michael Tonnes, and Mogens Lau

***Abstract* – More and more wind turbine manufacturers turn to use the full-scale power electronics converter due to the stricter grid code requirements in order to thoroughly decouple the generator from the grid connection. However, a common used type of the generator is still unclear, where the selections of the low-speed (direct-drive) and medium-speed (one-stage) permanent-magnet synchronous generators are both promising solutions. This paper will assess and compare the reliability metrics for the machine-side converter for those two configurations. First, a translation from the mission profile of the turbine to the current and voltage loading of the each power semiconductor is achieved based on the synchronous generator modeling. Afterwards, a simplified approach to calculate the loss profile and the thermal profile is used to determine the most stressed power semiconductors in the converter. Finally, according to the lifetime power cycles, the lifespan can be calculated when operating in various wind classes. It is concluded that, although the low-speed permanent-magnet synchronous generator is able to eliminate the gearbox, the lifespan of its machine-side converter is lower than the one-stage medium-speed generator.**

***Index Terms* – Power electronics converter, permanent-magnet synchronous generator, loss profile, thermal profile, lifetime prediction.**

I. INTRODUCTION

After the transition from the constant-speed squirrel-cage induction generator to the variable-speed generator, a number of generator types are adopted by the wind turbine manufacturers and the most optimum concept is still under discussion [1]-[5]. Initially, the wind turbine system equipped with the Doubly-Fed Induction Generator (DFIG) became attractive due to its traditional generator technology, having an affordable power converter as well as the fully controllability of the active and reactive power [6]. However, with the steady increase of the wind power penetration, grid codes are updated regularly and they have become stricter and stricter [7], [8], which prevents an overwhelming use of this partial-scale power converter based configuration, because of its poorer low voltage ride-through capability as discussed in [9], [10]. Correspondingly, more and more manufacturers turn to the solution based on the full-scale power converter, whereas the generator type is still uncertain. The options are the asynchronous Induction Generator (IG), the Electrically-Excited Synchronous Generator (EESG) and the Permanent-Magnet Synchronous Generator (PMSG) [11]. In the case of the PMSG application, the elimination of slip rings, a simpler gearbox and better grid support ability are the main advantages compared to the DFIG concept. Nevertheless, it will cause more expensive power electronic converters and higher loss dissipation in the power converters [12]. Simultaneously, the wind farms are moving from onshore to offshore to reduce the environmental impact and to obtain better wind conditions. Because of the high-cost operation and maintenance of the offshore wind farm, the lifespan of the wind turbine system preserves to be 20-25 years, which is much longer than the traditional industrial standard for power electronics products [13].

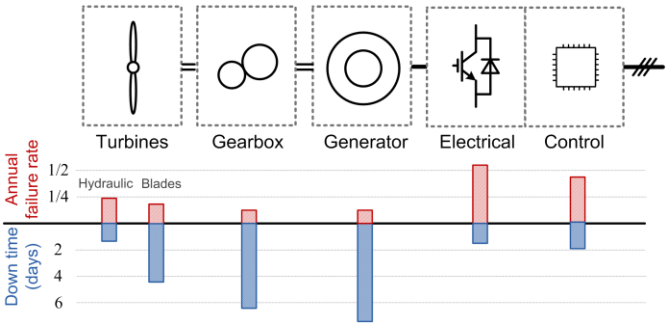

Fig. 1. Distribution of failure rate and down time for different parts in a wind turbine system [13].

Fig. 1 shows the distribution of failure rate and down time in a wind turbine system [13]. The power electronics component seems to have the highest failure rate, and its reliable operation becomes of interest from the manufacturer's perspective [13]-[17]. Moreover, Fig. 2 shows the stressors distribution in a power electronics system, and it is evident that the thermal stress is the dominant factor, which leads to most of the failure occurrence [18].

A lot of studies have already been carried out to assess the reliability of the power electronics components in wind power

Manuscript received August 26, 2014; revised December 9, 2014, and April 24, 2015; accepted May 21, 2015.

application [19]-[22]. As stated in [19], the lifespan of the wind power converter is estimated seen from the thermal cycling of the power component. However, the used concept of Mean Time To Failure (MTTF) is becoming outdated, as it does not take the real mission profile into account. The lifetime of the power device is analyzed by using multi-timescale of the mission profile in [20], but only the grid-side converter is focused and the characteristics of the wind power generator are not taken into account, which gives another thermal loading of the converter as the fundamental frequency is low and variable. Moreover, as stated in [21], the thermal cycling of the device can be induced either by the current commutation within one fundamental period or by the fluctuations of the wind speed as well as the ambient temperature. This paper addresses a general approach to estimate the lifetime of the machine-side converter in a wind power application. As the concepts of the low-speed and medium-speed PMSGs are becoming more widely used, the reliability assessment of both configurations is analyzed and compared seen from their estimated lifetime.

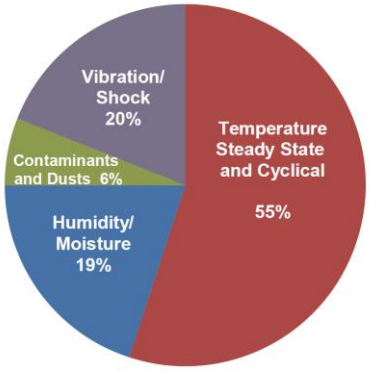

Fig. 2. Stressors distribution in a power electronics system which are affecting the reliability [18].

The paper is organized as follows. In section II, the focused topologies of the PMSGs and their modeling are addressed and described. Afterwards, section III and section IV deal with the analytical calculation of the loss profile and thermal profile. In accordance with the definition of the wind class, section V estimates and compares the lifetime of the power converters in various PMSG topologies. Finally, some concluding remarks are drawn in the last section.

II. Focused Generator Types

Although various generator types can be used to match a full-scale power converter, this paper is only interested in the direct-drive and one-stage gearbox PMSG systems, as they are the most used systems in industry.

A. System structures

Since the rotor speed of the direct-drive generator is the same as the turbine speed, a Low-Speed (LS) generator can be used. However, if a gearbox is preferred, the generator speed can be much faster than the turbine speed, by using a multi-stage gearbox for a High-Speed (HS) generator or a one-stage gearbox for a Medium-Speed (MS) generator. In respect to the multi-MW PMSGs, the systems are able to become one-stage or even direct-drive, which indicates that the rotor speed becomes low enough to match the turbine speed because of the dozens of pole pairs in the generators.

The configurations equipped with the LS and MS PMSGs are shown in Fig. 3(a) and Fig. 3(b), respectively. The full-scale Machine-Side Converter (MSC) and grid-side converter are linked together through the dc capacitor *C* in order to decouple the generator and the grid. It should be noted that different behaviors of the MSC can be expected due to the used generator types, while the grid-side converters of both systems perform the same characteristics. As a result, only the MSC is in focus in this paper. Moreover, a similar approach of the reliability assessment can be extended to the grid-side converter like discussed in [23].

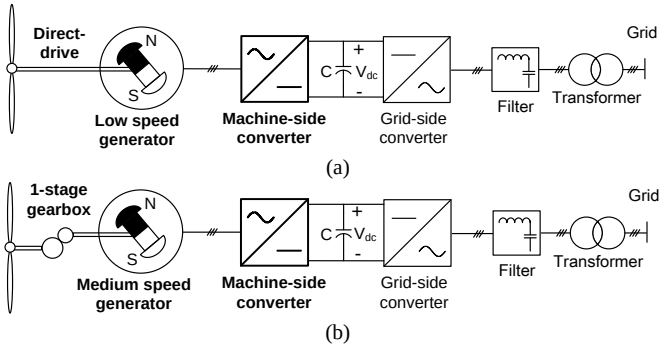

Fig. 3. Permanent-magnet synchronous generator based wind energy generation system. (a) Direct-drive with low-speed generator; (b) 1-stage gearbox with medium-speed generator.

B. Wind turbine

A 2 MW wind turbine is used as a case study in order to assess the systems, and the size is used for both the LS and MS PMSG systems. The most important parameters are listed in TABLE I [24]. It can be seen that the wind turbine generates electrical power from the cut-in wind speed at 3 m/s until the cut-off wind speed of 25 m/s, and the turbine speed varies from 6 rpm to 18 rpm, in which the wind speed at 12 m/s is regarded as the rated wind speed. Besides, the relationships of the turbine speed, output power in respect to the wind speed are shown in Fig. 4 [12], [24].

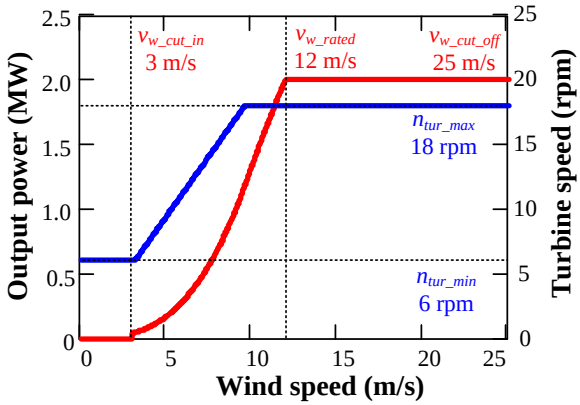

Fig. 4. Turbine speed and output power in respect to the wind speed.

TABLE I

PARAMETERS FOR 2 MW WIND TURBINE [24]

Rated power P_n [MW]	2.0
Blade radius R [m]	41.3
Cut-in wind speed $v_{w\_cut\text{-}in}$ [m/s]	3
Rated wind speed v_{w_rated} [m/s]	12
Cut-off wind speed $v_{w\_cut\_off}$ [m/s]	25
Optimal tip speed ratio λ_{opt}	8.1
Maximum power coefficient C_{pmax}	0.41
Maximum turbine speed n_{tur_max} [rpm]	18
Minimum turbine speed n_{tur_min} [rpm]	6

C. PMSG modeling

In order to achieve an independent control of the active and reactive power, d-axis and q-axis equivalent circuits are widely used in modern drive system. Regardless of the LS or the MS PMSG, it is modeled as shown in Fig. 5 [25], and the stator voltage at the d-axis u_{sd} and at the q-axis u_{sq} can be expressed as,

$$u_{sd} = R_s i_{sd} + L_s \frac{di_{sd}}{dt} - \omega_e L_s i_{sq} \tag{1}$$

$$u_{sq} = R_s i_{sq} + L_s \frac{di_{sq}}{dt} + \omega_e L_s i_{sd} + \omega_e \psi_m \tag{2}$$

where i_{sd} and i_{sq} denote the stator current in d-axis and q-axis, R_s and L_s denote the stator winding resistance and stator inductance, ω_e denotes the angular frequency of the stator current, and ψ_m denotes the rotor flux linkage.

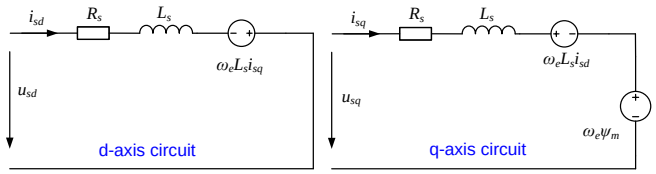

(a) (b)

Fig. 5. Steady-state equivalent circuit of the permanent-magnet synchronous generator. (a) d-axis circuit; (b) q-axis circuit.

As the rotor speed of the LS generator is very low to match the revolution of the wind turbine, a multi-pole structure makes this generator heavier and bulkier, which is a challenge because of the limited nacelle space. A tradeoff solution of MS generator can be realized by using a one-stage gearbox. Since its pole pairs are much less than the LS generator, it leads to a smaller size and lighter weight. The parameters of the LS and MS PMSGs are summarized in TABLE II, in which the pole pair of 26 appears in the LS generator, which is much higher than the 8 pole pairs of the MS generator. Moreover, due to the existence of gear-ratio in the MS generator, the frequency range of the LS generator stator current is only 2.6-7.8 Hz, which is much smaller than the MS generator of 16-48 Hz.

TABLE II

PARAMETERS FOR 2 MW LOW-SPEED (LS) AND MEDIUM-SPEED (MS) PMSGS [11], [26]

	LS Generator	***MS Generator***
Rated mechanical power P_s [MW]	2.0	2.0
Rated stator phase voltage U_s [V]	477	477
Rated stator current I_s [A]	3302	3302
Frequency range of stator current f_e [Hz]	2.6-7.8	16-48
Gear-ratio n_{gear}	/	20
Range of rotor speed n_r [rpm]	6-18	120-360
Number of pole pairs n_p	26	8
Rated rotor flux linkage ψ_m [Wb]	5.826 (rms)	0.947 (rms)
Stator winding resistance R_s [mΩ]	0.821	1.097
Stator inductance L_s [mH]	1.573	0.256

Although the application of the LS PMSG may avoid the existence of the gearbox, which is commonly considered as a fragile part of the wind turbine system, the paper is only focused on the reliability of power electronics converter. The flowchart to assess the reliability metrics of the power electronics components in the wind turbine system is shown in Fig. 6. The procedure starts with the analysis of the power profile in order to establish the relationship between the output power P_s and wind speed v_w. With the help of the PMSG model and the loss model for the power electronics components, the loss dissipation of the IGBT P_T and the diode P_D can be calculated according to the loading profile of the power converter. Based on the thermal model of the power module, the thermal profile of the power semiconductors can be calculated in terms of the mean junction temperature T_{jm} and the junction temperature fluctuation dT_j. Afterwards, the power cycles of the power semiconductor N_f can be obtained taking into account of the Coffin-Manson model as well as the on-state time effect. Finally, considering the mission profile (such as the wind speed distribution and wind class), the B_{10} lifetime of the power converter can be estimated.

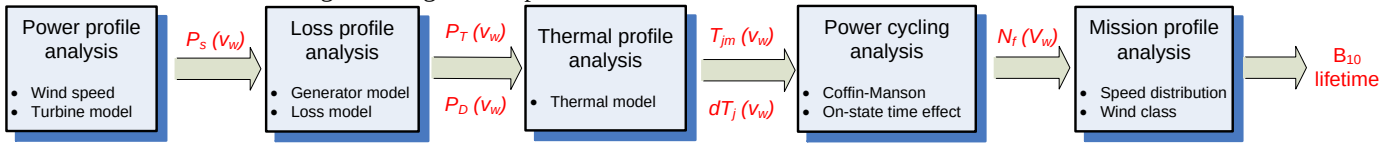

Fig. 6. Mission profile based approach to assess the reliability of a wind power converter.

III. Loss Profile Calculation

On the basis of the modeling of the PMSG, the loading profile of the machine-side converter equipped with LS and MS generators is evaluated and compared in terms of current, voltage as well as the displacement angle. Then, the loss dissipation for the machine-side converter with different generator types is analyzed and calculated.

A. Loading profile

In order to evaluate the loss dissipation, the loading profile of each power component needs to be calculated in advance. As a control scheme of Zero D-axis Current (ZDC) is usually preferred seen from the minimum generator copper loss [26], the amplitude of the stator current is solely determined by the q-axis current component, which can be calculated by the output power as shown in Fig. 4 over the q-axis stator voltage expressed in (2). Neglecting the voltage drop across the stator resistance and stator inductance, it can be stated that the stator voltage in q-axis is mainly caused by the Electro-Motive Force (EMF), which is the product of the stator angular frequency and the permanent-magnet rotor flux linkage. Correspondingly, the relationship between the stator current and the wind speed is shown in Fig. 7(a). It is noted that the stator current keeps increasing until the rated wind speed is reached. Moreover, the current characteristics between the LS and MS generators are almost the same because of a similar EMF calculated according to the relevant parameters listed in TABLE II. Furthermore, it can be seen that the maximum stator current at the rated wind speed already exceeds 3.0 kA. For state-of-the-art low voltage IGBT power module of 1 kA/1.7 kV, this rating cannot be realized without using a paralleled structure.

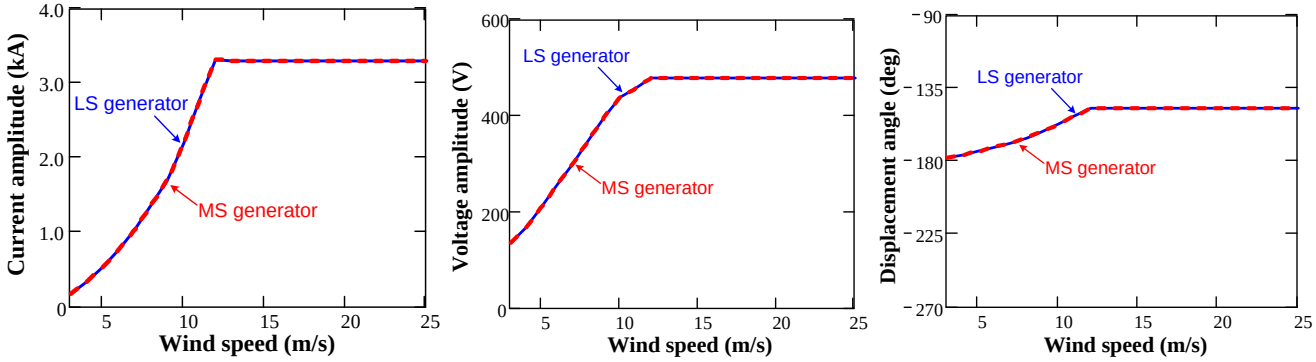

Fig. 7. Loading profile of machine-side converter with Low-Speed (LS) and Medium-Speed (MS) permanent-magnet synchronous generators. (a) Stator current; (b) Stator voltage; (c) Displacement angle.

Meanwhile, the generated q-axis current also contributes to the stator voltage in the d-axis as described in (1), and this component is minor compared to q-axis stator voltage. The stator voltage profiles of the LS and the MS generators are shown in Fig. 7(b), in which the similar behavior can still be observed. However, another turning point appears around the wind speed at 10 m/s. As shown in Fig. 4, the turbine speed obtains the maximum value above this wind speed, which also causes the maximum stator angular frequency. The constant value of the EMF induces the slow increase of the stator voltage because of a higher stator current as calculated in (2).

The displacement angles between the stator current and the stator voltage are then shown in Fig. 7(c). The displacement angle becomes almost -180 °at the cut-in wind speed, and the reason is that d-axis stator voltage is ignorable due to the relatively low stator current. With a higher wind speed, the higher stator current induces a higher d-axis stator voltage, which makes the displacement angle deviate from -180 °.

B. Loss calculation

The loss dissipation of the power switching device consists mainly of the conduction loss and the switching loss. As shown in Fig. 8, some relevant variables are required to be translated from the produced power by the Maximum Power Point Tracker (MPPT) of the wind turbine system. In order to eliminate the junction temperature influence to the power loss, the power loss information used from the datasheet is assumed to operate at maximum junction temperature (150 ℃) for the worst scenario. In respect to the conduction loss, if a Space Vector Modulation (SVM) with a symmetrical modulation sequence method of the no-zero vector and zero-vector are adopted under certain dc-link voltage [27], the stator voltage u_s and the displacement angle φ_s can be obtained through the PMSG model and can be used to estimate the duty cycle d for each switching pattern. Then, the conduction loss in each power device P_{con} can be calculated as [12],

$$P_{con} = f_e \cdot \Big(\sum_{n=1}^{N} V_{ce}\big(|i_a(n)|\big)\cdot|i_a(n)|\cdot d(n)T_s + \sum_{n=1}^{N} V_f\big(|i_a(n)|\big)\cdot|i_a(n)|\cdot(1-d(n))T_s \tag{3}$$

where the first term is the conduction loss of the IGBT P_{T_con}, and the second term is the conduction loss of the freewheeling diode P_{D_con}. i_a is the current through each power component, T_s is the switching period, V_{ce}, V_f are the voltage drop of the IGBT and the diode during their on-state period, which

normally are given by the manufacturer. N is the carrier ratio, whose value is the switching frequency f_s over the fundamental frequency f_e, and the subscript n is the nth switching pattern.

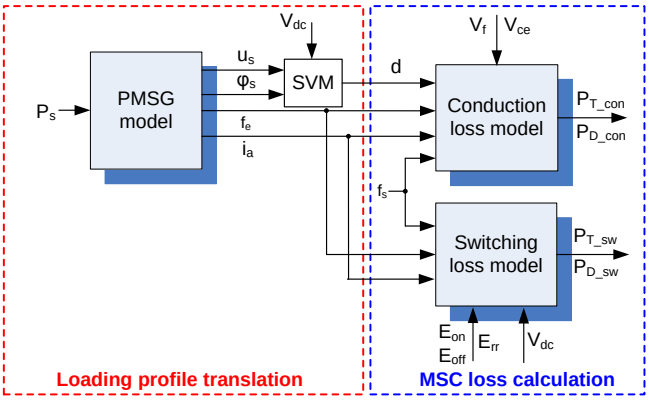

Fig. 8. Block diagram of loss calculation for Machine-Side Converter (MSC) equipped with Permanent-Magnet Synchronous Generator (PMSG).

The switching loss in each power device P_{sw} can be calculated as,

$$P_{sw} = \frac{V_{dc}}{V_{dc}^*} \cdot f_e \cdot \left(\sum_{n=1}^{N} \left(E_{on}\left(|i_a(n)|\right) + E_{off}\left(|i_a(n)|\right)\right) + \sum_{n=1}^{N} E_{rr}\left(|i_a(n)|\right)\right) \quad (4)$$

The first term is the switching loss for the IGBT P_{T_sw}, and the second term is the switching loss for the freewheeling diode P_{D_sw}. E_{on} and E_{off} are the turn-on and the turn-off energy dissipated by the IGBT, and E_{rr} is the reverse-recovery energy dissipated by the diode, which normally are given by the manufacturer at a certain dc-link voltage V_{dc}^*. It is assumed that the switching energy is proportional to the actual dc-link voltage V_{dc}. In order to calculate the switching loss, only the information about the stator current and its frequency are needed.

TABLE III

PARAMETERS FOR MACHINE-SIDE CONVERTERS EQUIPPED WITH LOW-SPEED (LS) AND MEDIUM-SPEED (MS) PMSGS

	LS Generator	***MS Generator***
Frequency of stator current f_e [Hz]	2.6-7.8	16-48
Period of stator current t_e [ms]	128.2-384.6	20.8-62.5
Power modules used in each MSC leg	1 kA/1.7 kV; four in parallel	
Switching frequency f_s [kHz]	2	
Switching period T_s [μs]	500	
Reference dc-link voltage V_{dc}^* [V]	900	
Switching frequency V_{dc} [V]	1050	

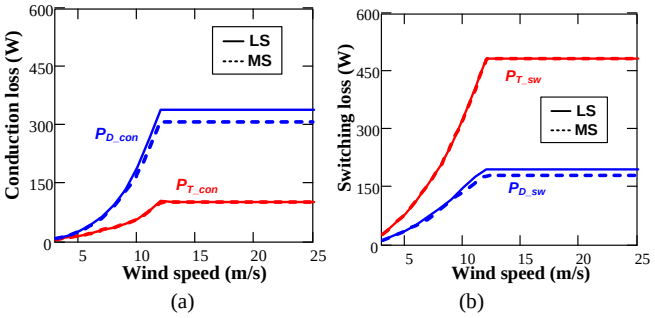

Fig. 9. Loss comparison of IGBT and freewheeling diode in each power switch with Low-speed (LS) and Medium-Speed (MS) generators. (a) Conduction loss; (b) Switching loss.

With the important parameters listed in TABLE III, the losses of the IGBT and the diode in each power switch are compared in Fig. 9 with the LS and the MS generators. Regarding the conduction loss, the freewheeling diode is having more power dissipation than the IGBT due to the fact that the power is flowing from the synchronous generator into the dc-link and then fed into the grid. For the switching loss, because of the higher switching energy in the IGBT chip, the diode has the lowest loss dissipation. Moreover, an equal loss breakdown of the LS and MS generator systems are observed due to the same loading profile and switching frequency. Afterwards, the total loss of the IGBT P_T and diode P_D are shown in Fig. 10. It is noted that, regardless of the LS and the MS generators, the loss dissipation of the IGBT and the diode are almost similar. A slight difference occurs in the diode due to the various fundamental frequencies of the generators.

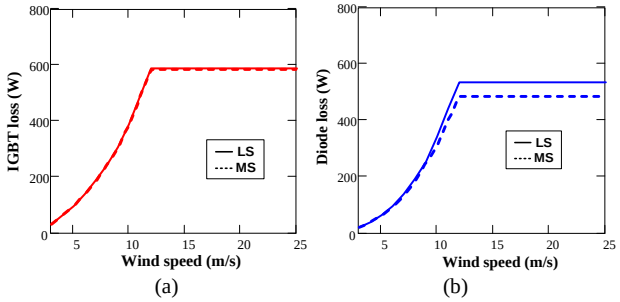

Fig. 10. Loss profile of various components equipped with Low-Speed (LS) and Medium-Speed (MS) generators. (a) IGBT; (b) Freewheeling diode.

IV. THERMAL PROFILE CALCULATION

Based on the loss dissipation calculated in section III, this section will further discuss and evaluate the thermal stress of the power semiconductor devices.

A. Thermal model

Two kinds of thermal network are commonly adopted to model the thermal behavior: the more physical-meaning based Cauer structure and the experimental-result based Foster structure. The latter is actually more preferred by the industry [28], [29]. It is the thermal impedance that decides the junction temperature of the power device, which usually consists of the power module itself (from junction to baseplate

or case), the Thermal Interface Material (TIM) as well as the cooling method, as shown in Fig. 11.

Generally, the thermal time constant of a typical air cooled system is from dozens to hundreds of seconds for MW-level power converter, while the maximum thermal time constant of the power module itself is hundreds of milliseconds. On the other hand, the maximum fundamental period of the MSC output current is only hundreds of milliseconds in the case that the LS PMSG is used, which implies that the thermal cycling caused by the air cooling can almost be neglected [29], [30]. As a result, for the steady-state thermal cycle, the thermal model of the cooling method will only affect the mean junction temperature, but it will not disturb the junction temperature fluctuation.

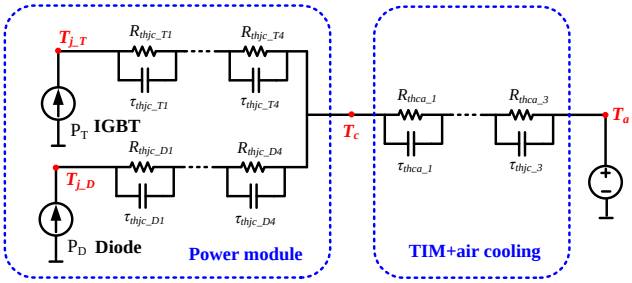

Fig. 11. Thermal model of power module, in which both the IGBT chip and diode chip are taken into account (TIM: Thermal Interface Material).

B. Thermal cycling

The mean junction temperature T_{jm} and the junction temperature fluctuation dT_j are normally regarded as the two most important reliability stressors, and the formulae to calculate them are [31], [32],

$$T_{jm\_T/D} = P \cdot \sum_{i=1}^{4} R_{thjc\_T/D(i)} + P \cdot \sum_{j=1}^{3} R_{thca\_(j)} + T_a \tag{5}$$

$$dT_{j\_T/D} = 2P \cdot \sum_{i=1}^{4} R_{thjc\_T/D(i)} \cdot \frac{(1-e^{-\frac{t_{on}}{\tau_{thjc\_T/D(i)}}})^2}{1-e^{-\frac{t_e}{\tau_{thjc\_T/D(i)}}}} \tag{6}$$

In (5), R_{thjc} is the thermal resistance from the junction to case of the power module, R_{thca} is the thermal resistance of the air cooling system, in which subscripts T and D denote the IGBT and the freewheeling diode, whereas subscripts i and j denote four-layer and three-layer Foster structure for power module and air cooling, respectively. P is the power loss of each power semiconductor, and T_a is the ambient temperature. In (6), t_{on} denotes the on-state time within each fundamental period of the current at the steady-state operation, t_e denotes the fundamental period of the current, τ denotes the thermal time constant of each Foster layer.

According to (5) and (6), and together with the loss profile shown in Fig. 10, the thermal profile of the IGBT and the diode can be calculated for the wind turbine operation as shown in Fig. 12. In respect to the mean junction temperature, although a similar loss dissipation of the IGBT and the diode can be found in Fig. 10, the diode has a higher mean junction temperature due to its higher thermal resistance caused by smaller chip size.

For the junction temperature fluctuation, as it is illustrated in (6), the amplitude of the thermal cycling is closely related to the power loss and the fundamental period of the stator current. As the similar power loss of the IGBT and diode can be found between the LS and MS generator like shown in Fig. 10, a lower fundamental frequency of the LS generator leads to a higher thermal cycling. In brief, it can be seen that the diode is the most stressed in terms of the mean junction temperature and the junction temperature fluctuation for both the LS and MS generator systems.

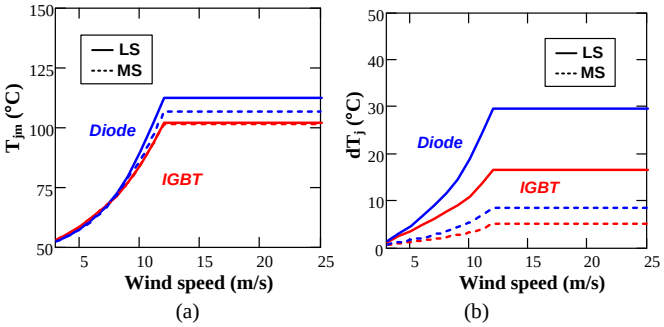

Fig. 12. Thermal profile of the machine-side converter equipped with Low-Speed (LS) and Medium-Speed (MS) generators. (a) Mean junction temperature; (b) Junction temperature fluctuation.

V. LIFETIME CALCULATION

This section introduces a method to estimate the lifetime of the power converter and compares the lifetime of the LS and MS PMSG systems, in which the assumptions for the reliability evaluation are also addressed.

The power electronics reliability involves multidisciplinary knowledge, which covers the analytical physics to understand the failure mechanisms of power electronics products; the design for reliability and robustness validation process to build in reliability and sufficient robustness during the development process of the power electronics device; as well as intelligent control and condition monitoring to ensure reliable field operation under specific mission profile [33]. Consequently, the lifetime estimation for the power semiconductor device is not an easy task, and the following assumptions are made,

a. Although the bond-wire liftoff and the soldering cracks between the different layers occur frequently in power modules due to fatigue [28], [32], a unified failure mechanism is assumed in this study;

b. The Miner's rule is used for the lifetime calculation [35], which means that a linear damage accumulation in the fatigue is assumed, and the component parameters will seldom deviate along with the system operation;

c. As most of the manufacturers cannot provide the numbers of power cycling with small temperature swing and high cycling frequency, extended data is obtained through the conventional Coffin-Manson lifetime model [37];

d. The confidence level due to parameter variation is not of concern in this paper, and the used B_{10} lifetime model specifies that if the power cycles reach the specific value, 10% of the total sampling devices will be damaged [34].

In order to calculate the power cycles of the power semiconductor, the Coffin-Manson formula is used [32], [36],

$$N_f = A \cdot dT_j^{\alpha} \cdot \exp\left(\frac{E_a}{k_b \cdot T_{jm}}\right) \tag{7}$$

It can be seen that the power cycles are closely related to the junction temperature fluctuation dT_j and the mean junction temperature T_{jm}. Moreover, E_a and k_b denote activation energy and Boltzmann constant, respectively [32]. α and A are obtained according to test data of power modules provided by the manufacturer.

According to [32], the on-state time within each fundamental period t_{on} is also closely relevant to the power cycling capability, and this factor should be taken into account as well,

$$\frac{N_f(t_{on})}{N_f(0.7s)} = \left(\frac{t_{on}}{0.7s}\right)^{-0.463} \tag{8}$$

Based on (7) and (8), the strength model of the power semiconductor device can roughly be estimated (i.e. the number of the power cycles can be undertaken before the failure occurs). The relationship between the lifetime power cycles and the wind speed is shown in Fig. 13(a), in which the LS and MS generators both are involved. Compared with the IGBT and the diode chip, it is evident that the diode has lower B_{10} lifetime power cycles due to its higher mean junction temperature as well as the junction temperature fluctuation. Moreover, since the LS PMSG has an even higher mean junction temperature and larger junction temperature swing, it is noted that the LS generator has lower power cycles at all operational wind speeds, which is consistent with (7).

Nevertheless, the manufacturers are more concerned about the lifespan of the system, and the mission profile is important for the stress analysis. For a wind energy conversion system, it can almost be regarded that the wind profile appears periodical every year, the annual Consumed Lifetime (*CL*) can be calculated by dividing the total number of cycles per year by the B_{10} lifetime estimated by (7) and (8),

$$CL_m = D_m \cdot \frac{365 \cdot 24 \cdot 3600 \cdot f_{e\_m}}{N_{f\_m}} \tag{9}$$

where D is the annual percentage of the every wind speed, f_e is the fundamental frequency of the stator current, and N_f is the B_{10} lifetime power cycles. Subscript m denotes the various wind speeds from the cut-in to the cut-off wind speed. According to the IEC standard [38], three various wind categories - Class I, Class II and Class III can be used, whose average wind speeds are 10 m/s, 8.5 m/s and 7.5 m/s, respectively. If the wind Class I is applied by using Weibull distribution of the wind speed [39], the annual consumed lifetime can be calculated and it is graphically shown in Fig. 13(b). Although the LS generator has a lower fundamental frequency, the consumed lifetime of the LS generator is higher than the MS generator due to the much lower B_{10} power cycles of the LS generator.

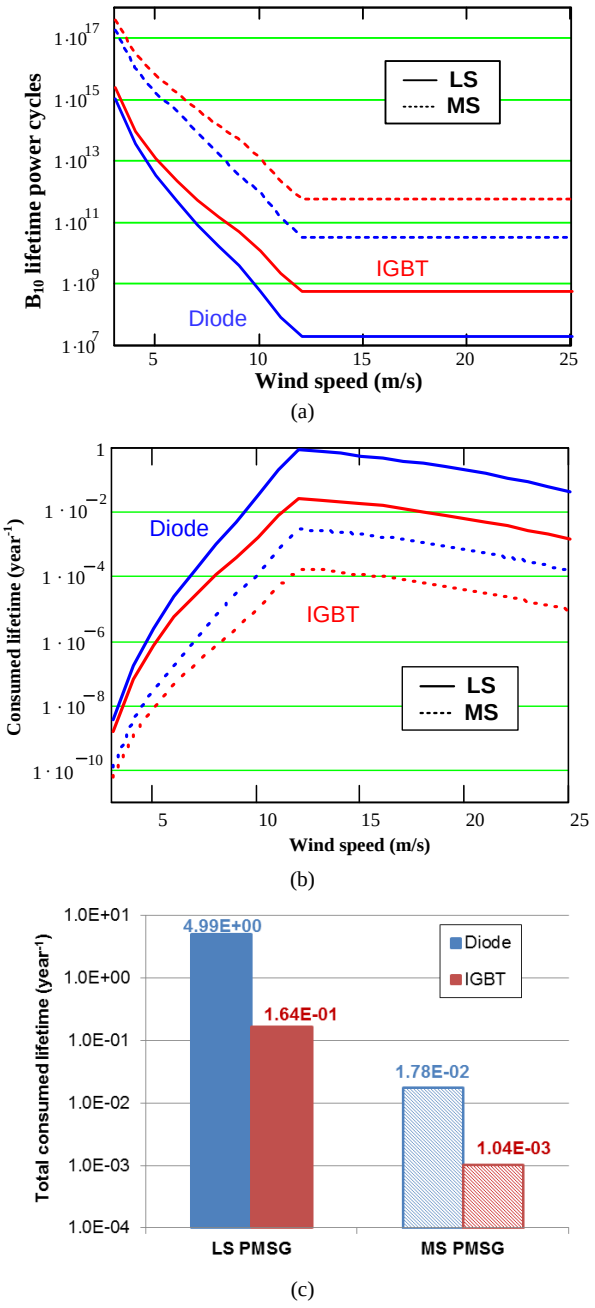

Fig. 13. Lifetime comparison of power semiconductors used in power electronics converter of Low-Speed (LS) and Medium-Speed (MS) generators. (a) B_{10} lifetime power cycles; (b) Consumed lifetime at individual wind speed; (c) Total consumed lifetime.

As shown in Fig. 14, the procedure to estimate the lifetime of the wind power converter is comprehensively illustrated from the mission profile to reliability metrics. The Total Consumed Lifetime (*TCL*) can then be estimated by the decomposition of the wind speed in terms of a wind speed increment of 1 m/s,

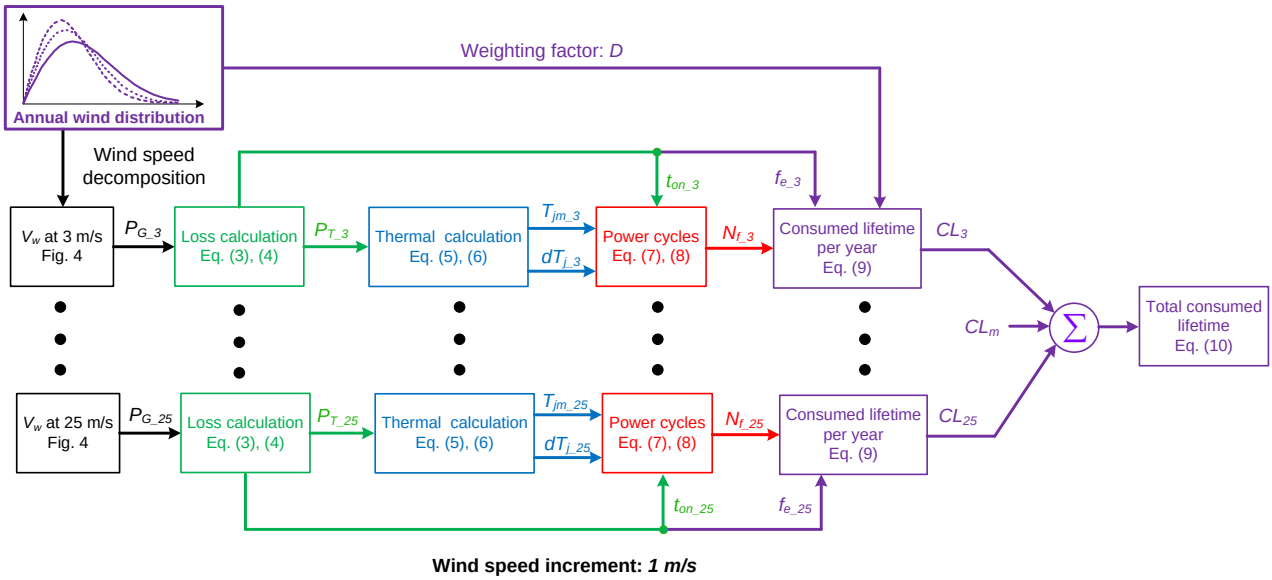

Fig. 14. Block diagram to calculate lifetime based on an annual wind profile in a wind turbine.

$$TCL = \sum_{n=3}^{25} CL_n \tag{10}$$

As shown in Fig. 13(c), the lifetime of the diode chip and the IGBT chip are compared, and it indicates that the IGBT lifetime is at least 10 times higher than the diode regardless of the LS or MS PMSG. As a consequence, it is fair to assume that the lifetime of the MSC is determined by the diode, and in the following lifetime estimation of the power converter will only focus on the diode chip.

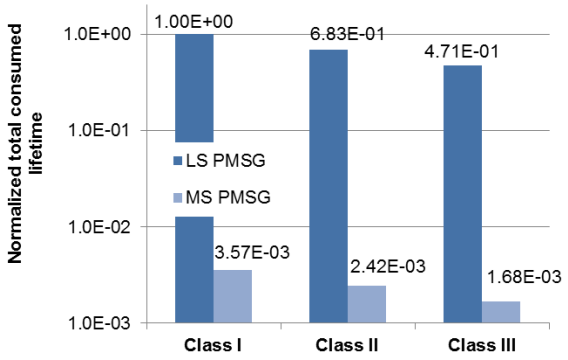

Fig. 15. Normalized total consumed lifetime between Low-Speed (LS) and Medium-Speed (MS) generators with various wind classes.

As shown in Fig. 15, the normalized total consumed lifetime between the MSCs of the LS and the MS generators are compared with various wind classes, where the lifetime of the LS generator at wind class I is regarded as the base value. It is obvious that, regardless of the wind class, the lifetime of the LS generator becomes much lower compared to the MS generator application. For instance, if a Class I wind profile is selected, the annual lifetime consumption of the LS generator is 1.00E+00 and the MS generator is 3.57E-3, which implies that the lifespan of the MS generator system is almost 300 times higher than the LS generator system. Besides, if different wind classes are used, the tendency of the lifetime distribution appears almost to be the same.

VI. Conclusion

This paper describes and addresses a universal method to calculate lifetime for the power electronics converter equipped with low-speed and medium-speed permanent-magnet synchronous generators. First, the translation from the mission profile to the current and voltage loading of the each power semiconductor can be achieved based on the synchronous generator modeling. Afterwards, a simplified approach to calculate the loss profile and the thermal profile can determine the most stressed power semiconductor (the IGBT or the freewheeling diode). Finally, according to the modeling of the B_{10} lifetime power cycles, the lifespan can be deduced and compared with various wind classes. It is concluded that, the lifespan of machine-side converter equipped with low-speed permanent-magnet synchronous generator is much lower than the one-stage medium-speed generator, since the thermal cycling of the low-speed generator becomes much higher due to its lower operational frequency. To overcome this issue, a higher rating of the power converter may be required for the low-speed generator for the similar lifespan of the machine-side converter equipped with the medium-speed generator. However, the reliability metrics of the medium-speed generator may be compromised seen from the system point of view due to the existence of the gearbox.

References

[1] F. Blaabjerg, and K. Ma, "Future on power electronics for wind turbine systems," *IEEE Trans. Emerg. Sel. Topics Power Electron.*, vol. 1, no. 3, pp. 139-152, Sep. 2013.

[2] H. Polinder, J. A. Ferreira, B. B. Jensen, AB. Abrahamsen, K. Atallah, and R. A. McMahon, "Trends in wind turbine generator systems," *IEEE Trans. Emerg. Sel. Topics Power Electron.*, vol. 1, no. 3, pp.174-185, Sep. 2013.

[3] M. Liserre, R. Cardenas, M. Molinas, and J. Rodriguez, "Overview of multi-MW wind turbines and wind parks," *IEEE Trans. Ind. Electron.*, vol. 58, no. 4, pp. 1081-1095, Apr. 2011.

[4] J. M. Guerrero, F. Blaabjerg, T. Zhelev, K. Hemmes, E. Monmasson, S. Jemei, M. P. Comech, R. Granadino, and J. I. Frau, "Distributed generation: toward a new energy paradigm," *IEEE Ind. Electron. Mag.*, vol. 4, no. 1, pp. 52-64, Mar. 2010.

[5] D. Zhou, F. Blaabjerg, T. Franke, M. Tonnes, and M. Lau, "Reduced cost of reactive power in doubly fed induction generator wind turbine system with optimized grid filter," *IEEE Trans. Power Electron.*, vol. 30, no. 10, pp. 5581-5590, Oct. 2015.

[6] R. Cardenas, R. Pena, S. Alepuz, and G. Asher, "Overview of control systems for the operation of DFIGs in wind energy applications," *IEEE Trans. Ind. Electron.*, vol. 60, no. 7, pp. 2776-2798, Jul. 2013.

[7] E.ON-Netz. Requirements for offshore grid connections, Apr. 2008.

[8] M. Tsili, and S. Papathanassiou, "A review of grid code technical requirements for wind farms," *IET Renewable Power Generation*, vol. 3, no. 3, pp. 308-332, Sep. 2009.

[9] S. Xiao, G. Yang, H. Zhou, and H. Geng, "An LVRT control strategy based on flux linkage tracking for DFIG-based WECS," *IEEE Trans. Ind. Electron.*, vol. 60, no. 7, pp. 2820-2832, Jul. 2013.

[10] J. Lopez, E. Gubia, E. Olea, J. Ruiz, and L. Marroyo, "Ride through of wind turbines with doubly fed induction generator under symmetrical voltage dips," *IEEE Trans. Ind. Electron.*, vol. 56, no. 10, pp. 4246-4254, Oct. 2009.

[11] J. Chivite-Zabalza, C. Girones, A. Carcar, I. Larrazabal, E. Olea, and M. Zabaleta, "Comparison of power conversion topologies for a multi-megawatt off-shore wind turbine, based on commercial power electronic building blocks," *in Proc. of IECON 2013*, pp. 5242-5247, 2013.

[12] D. Zhou, F. Blaabjerg, M. Lau, and M. Tonnes, "Thermal analysis of multi-MW two-level wind power converter," *in Proc. of IECON 2012*, pp. 5858-5864, 2012.

[13] B. Hahn, M. Durstewitz, and K. Rohrig "Reliability of wind turbines - Experience of 15 years with 1500 WTs," *Wind Energy: Proceedings of the Euromech Colloquium*, pp. 329-332, Springer-Verlag, Berlin.

[14] C. Busca, R. Teodorescu, F. Blaabjerg, S. Munk-Nielsen, L. Helle, T. Abeyasekera, and P. Rodriguez, "An overview of the reliability prediction related aspects of high power IGBTs in wind power applications," *Microelectronics Reliability*, vol. 51, no. 9-11, pp. 1903-1907, 2011.

[15] S. Yang, A. Bryant, P. Mawby, D. Xiang, L. Ran, and P. Tavner, "An industry-based survey of reliability in power electronic converters," *IEEE Trans. Ind. Appl.*, vol. 47, no. 3, pp. 1441-1451, May-June 2011.

[16] F. Richardeau, and T. T. L. Pham, "Reliability calculation of multilevel converters: theory and applications," *IEEE Trans. Ind. Electron.*, vol. 60, no. 10, pp. 4225-4233, Oct. 2013.

[17] H. Behjati, and A. Davoudi, "Reliability analysis framework for structural redundancy in power semiconductors," *IEEE Trans. Ind. Electron.*, vol. 60, no. 10, pp. 4376-4386, Oct. 2013.

[18] ZVEL, Handbook for robustness validation of automotive electrical/electronic modules, Jun. 2008.

[19] L. Wei, R. J. Kerkman, R. A. Lukaszewski, H. Lu, and Z. Yuan, "Analysis of IGBT power cycling capabilities used in doubly fed induction generator wind power system," *IEEE Trans. Ind. Appl.*, vol. 47, no. 4, pp. 1794-1801, Jul. 2011.

[20] K. Ma, M. Liserre, F. Blaabjerg, and T. Kerekes, "Thermal loading and lifetime estimation for power device considering mission profiles in wind power converter," *IEEE Trans. Power Electron.*, vol. 30, no. 2, pp. 590-602, Feb. 2015.

[21] D. Weiss, and H. Eckel, "Fundamental frequency and mission profile wearout of IGBT in DFIG converters for wind power", *in Proc. of EPE 2013*, pp. 1-6, 2013.

[22] N. Patil, D. Das, and M. Pecht, "A prognostic approach for non-punch through and field stop IGBTs," *Microelectronics Reliability*, vol. 52, no. 3, pp. 482–488, 2012.

[23] D. Zhou, F. Blaabjerg, M. Lau, and M. Tonnes, "Optimized reactive power flow of DFIG power converters for better reliability performance considering grid codes," *IEEE Trans. Ind. Electron.*, vol. 62, no. 3, pp. 1552-1562, Mar. 2015.

[24] Enercon E-82 wind turbine. (Website: www.enercon.de/en-en/62.htm).

[25] H. Polinder, F. F. A. van der Pijl, G.-J. de Vilder, and P. J. Tavner, "Comparison of direct-drive and geared generator concepts for wind turbines," *IEEE Trans. Energy Convers.*, vol. 21, no. 3, pp. 725-733, Sep. 2006.

[26] B. Wu, Y. Lang, N. Zargari, and S. Kouro, Power conversion and control of wind energy systems. Piscataway, NJ: IEEE Press, 2011.

[27] K. Zhou, and D. Wang, "Relationship between space-vector modulation and three-phase carrier-based PWM: a comprehensive analysis," *IEEE Trans. Ind. Electron.*, vol. 49, no. 1, pp. 186-196, Feb. 2002.

[28] R. Schnell, M. Bayer, and S. Geissmann, "Thermal design and temperature ratings of IGBT modules," ABB Application Note, 5SYA 2093-00, 2011.

[29] T. Schutze, "Thermal equivalent circuit models," Infineon Application Note, AN2008-03, 2008.

[30] D. Zhou, F. Blaabjerg, M. Lau, and M. Tonnes, "Thermal cycling overview of multi-megawatt two-level wind power converter at full grid code operation," *IEEJ Journal of Industry Applications*, vol. 2, no. 4, pp. 173-182, Jul. 2013.

[31] D. Zhou, F. Blaabjerg, M. Lau, and M. Tonnes, "Thermal profile analysis of doubly-fed induction generator based wind power converter with air and liquid cooling methods," *in Proc. of EPE 2013*, pp.1-10, 2013.

[32] A. Wintrich, U. Nicolai, and T. Reimann, "Semikron Application Manual," 2011.

[33] H. Wang, M. Liserre, F. Blaabjerg, P. de Place Rimmen, J. B. Jacobsen, T. Kvisgaard, and J. Landkildehus, "Transitioning to physics-of-failure as a reliability driver in power electronics," *IEEE Trans. Emerg. Sel. Topics Power Electron.*, vol. 2, no. 1, pp. 97-114, Mar. 2014.

[34] ABB Application Note, Load-cycling capability of HiPak IGBT modules, 2012.

[35] M. A. Miner, "Cumulative damage in fatigue," *Journal of Applied Mechanics*, no. 12, A159-A164, 1945.

[36] E. Sutrisno, Q. Fan, D. Das, and M. Pecht, "Anomaly detection for Insulated Gate Bipolar Transistor (IGBT) under power cycling using principal component analysis and K-Nearest neighbor algorithm," *Journal of the Washington Academy of Sciences*, 2012.

[37] R. Amro, J. Lutz, and A. Lindemann, "Power cycling with high temperature swing of discrete components based on different technologies," *in Proc. of PESC 2004*, pp. 2593-2598, 2004.

[38] Wind turbines – part I: design requirements", IEC 61400-1, 3rd edition.

[39] The Swiss wind power data website. (Website: http://wind-data.ch/tools/weibull.php)

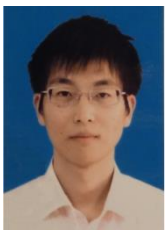

Dao Zhou (S'12, M'15) received the B.Sc. in electrical engineering from Beijing Jiaotong University, Beijing, China, in 2007, and the M. Sc. in power electronics from Zhejiang University, Hangzhou, China, in 2010. He received the Ph.D degree in the Department of Energy Technology, Aalborg University, Denmark, in 2014, where he is currently working as a Postdoc.

His research interests include power electronics

converters and their application and reliability in wind power generation systems.

Frede Blaabjerg (S'86-M'88-SM'97-F'03) was with ABB-Scandia, Randers, Denmark, from 1987 to 1988. From 1988 to 1992, he was a PhD student with Aalborg University, Aalborg, Denmark. He became an Assistant Professor in 1992, an Associate Professor in 1996, and a Full Professor of power electronics and drives in 1998. His current research interests include power electronics and its applications such as in wind turbines, PV systems, reliability, harmonics and adjustable speed drives.

He has received 15 IEEE Prize Paper Awards, the IEEE PELS Distinguished Service Award in 2009, the EPE-PEMC Council Award in 2010, the IEEE William E. Newell Power Electronics Award 2014 and the Villum Kann Rasmussen Research Award 2014. He was an Editor-in-Chief of the IEEE TRANSACTIONS ON POWER ELECTRONICS from 2006 to 2012. He has been Distinguished Lecturer for the IEEE Power Electronics Society from 2005 to 2007 and for the IEEE Industry Applications Society from 2010 to 2011.

Toke Franke (M'11) received the Dipl.-Ing. and Ph.D. degrees from Christian-Albrechts-University, Kiel, Germany in 2007 and 2013, respectively.

Between 2007 and 2011 he carried out research work at Christian-Albrechts-University on silicon carbide power devices in solar applications.

From 2011 to 2013 he was senior hardware technology engineer at Danfoss Solar Inverters there he focused on storage technologies and silicon carbide power devices. In 2014 he joined Danfoss Silicon Power as senior engineer for power stacks. His main research interest includes power devices and high density power stacks for renewable energies.

Dr. Franke is member of the IEEE Power Electronics Society.

Michael Tonnes received the M.Sc. EE degree from Aalborg University, Denmark in 1987, and the Ph.D. degree from the Institute of Energy Technology in 1990.

He was employed by Danfoss in 1987 to perform the Ph.D work within auto-tuning and automatic control of non-linear electrical machines and worked within the technology area of Motor Controls. Michael worked in US in Danfoss High Power Drives for the period 1996-98 and had various management positions within electronic businesses. At present he is Senior Director of R&D at Danfoss Silicon Power GmbH with base in Flensburg, Germany.

He is author and co-author on a number of articles within auto-tuning, motor controls and power electronics in general and holds several patents within the field motor controls and power electronics.

Mogens Lau received the M.Sc. in Electrical engineering from Aalborg University, Aalborg, Denmark, in 1999. He worked as development engineer, project manager and line manager within power electronics at leading companies like Siemens, Danfoss, Grundfoss and Vestas. Currently, he is the working with Siemens Wind Power A/S in Brande, Denmark.